1. INTRODUCTION—D. S. Arndt, J. Blunden, and K. M. Willett

This is the 26th edition of the annual assessment now known as *State of the Climate*. The year 2015 saw the toppling of several symbolic mileposts: notably, it was 1.0°C warmer than preindustrial times, and the Mauna Loa observatory recorded its first annual mean carbon dioxide concentration greater than 400 ppm. Beyond these more recognizable markers, changes seen in recent decades continued.

The year's exceptional warmth was fueled in part by a nearly year-round mature El Niño event, which is an omnipresent backdrop to the majority of the sections in this edition.

The ENSO phenomenon is perhaps the most visible reminder of connections across regions, scales, and systems. It underscores the circumstance that the climate system's components are intricately connected, to each other and to the world's many natural and human systems.

To that end, this year's SoC has an emphasis on ecosystems; several chapters have dedicated a sidebar to the complex relationship between a changing climate and its impact on living systems. This notion of connectedness—between climate, landscape, and life; between our daily work and the expression of its meaning; between planetary-scale drivers and humble living things; between the abstraction and rigor of data and the reality and complexity of their importance; and especially between one generation and the next—inspires and informs much of the work within this volume.

Our cover images this year reflect these intimate connections. Many of the shapes in the images are drawn, quite literally, from time series represented in this volume. The artist, Jill Pelto, is a practicing Earth scientist whose work reflects her field experience and her interpretation of the connection between global change, landscape, and life. Her father, Mauri, is both a longtime contributor to the *State of the Climate* series and a steward of a prominent global glacier dataset.

To convey these connections so beautifully and generously is a gift; we are thankful to artist and scientist alike, for sharing their talents and disciplines with the community.

Finally, we wish one of our dearest and most valuable connections, our technical editor, Mara Sprain, a speedy recovery from an unexpected health challenge. Her consistency and diligence continue to be a model for this series.

An overview of findings is presented in the Abstract, Fig. 1.1, and Plate 1.1. Chapter 2 features global-scale climate variables; Chapter 3 highlights the global oceans; and Chapter 4 includes tropical climate phenomena including tropical cyclones. The Arctic and Antarctic respond differently through time and are reported in separate chapters (5 and 6, respectively). Chapter 7 provides a regional perspective authored largely by local government climate specialists. Sidebars included in each chapter are intended to provide background information on a significant climate event from 2015, a developing technology, or an emerging dataset germane to the chapter's content. A list of relevant datasets and their sources for all chapters is provided as an Appendix.

Time series of major climate indicators are again presented in this introductory chapter. Many of these indicators are essential climate variables (ECVs), originally defined in GCOS 2003 and updated again by GCOS in 2010.

The following ECVs, included in this edition, are considered "fully monitored," in that they are observed and analyzed across much of the world, with a sufficiently long-term dataset that has peer-reviewed documentation:

- Atmospheric Surface: air temperature, precipitation, air pressure, water vapor, wind speed and direction.
- Atmospheric Upper Air: earth radiation budget, temperature, water vapor, wind speed and direction.
- Atmospheric Composition: carbon dioxide, methane, other long-lived gases, ozone.
- Ocean Surface: temperature, salinity, sea level, sea ice, current, ocean color, phytoplankton.
- Ocean Subsurface: temperature, salinity.
- Terrestrial: snow cover, albedo.

ECVs in this edition that are considered "partially monitored," meeting some but not all of the above requirements, include:

- Atmospheric Upper Air: cloud properties.
- Atmospheric Composition: aerosols and their precursors.
- Ocean Surface: carbon dioxide, ocean acidity.
- Ocean Subsurface: current, carbon.
- Terrestrial: soil moisture, permafrost, glaciers and ice caps, river discharge, groundwater, ice sheets, fraction of absorbed photosynthetically active radiation, biomass, fire disturbance.

Remaining ECVs that are desired for the future include:

- Atmospheric Surface: surface radiation budget.
- Ocean Surface: sea state.
- Ocean Subsurface: nutrients, ocean tracers, ocean acidity, oxygen.
- Terrestrial: water use, land cover, lakes, leaf area index, soil carbon.

PLATE 1.1. Global (or representative) average time series for essential climate variables. Anomalies are shown relative to the base period in parentheses although original base periods (as shown in other sections of the report) may differ. The numbers in the square brackets that follow in this caption indicate how many reanalysis (blue), satellite (red), and in situ (black) datasets are used to create each time series in that order. (a) N. Hemisphere lower stratospheric ozone (March) [0,5,1]; (b) S. Hemisphere lower stratospheric ozone (October) [0,5,1]; (c) Apparent transmission (Mauna Loa) [0,0,1]; (d) Lower stratospheric temperature [3,3,4]; (e) Lower tropospheric temperature [3,2,4]; (f) Surface temperature [4,0,4]; (g) Extremes (warm days (solid) and cool nights (dotted)) [0,0,1]; (h) Arctic sea ice extent (max (solid) and min (dashed)) [0,0,2]; (i) Antarctic sea ice extent (max (solid) and min (dashed)) [0,0,2]; (j) Glacier cumulative mean specific balance [0,0,1]; (k) N. Hemisphere snow cover extent [0,1,0]; (l) Lower stratospheric water vapor [0,1,0]; (m) Cloudiness [1,6,1]; (n) Total column water vapor–land [0,1,2]; (o) Total column water vapor–ocean [0,2,0]; (p) Upper Tropospheric Humidity [1,1,0]; (q) Specific humidity–land [3,0,4]; (r) Specific humidity–ocean [3,1,3]; (s) Relative humidity–land [2,0,4]; (t) Relative humidity–ocean [2,0,2]; (u) Precipitation–land [0,0,3]; (v) Precipitation–ocean [0,3,0]; (w) Ocean heat content (0–700 m) [0,0,4]; (x) Sea level rise [0,1,0]; (y) Tropospheric ozone [0,1,0]; (z) Tropospheric wind speed at 300 hPa for 20°–40°N [5,0,1]; (aa) Land wind speed [0,0,2]; (ab) Ocean wind speed [4,1,2]; (ac) Biomass burning [0,2,0]; (ad) Soil moisture [0,1,0]; (ae) Terrestrial groundwater storage [0,1,0]; (af) FAPAR [0,1,0]; (ag) Land surface albedo–visible (solid) and infrared (dashed) [0,2,0].

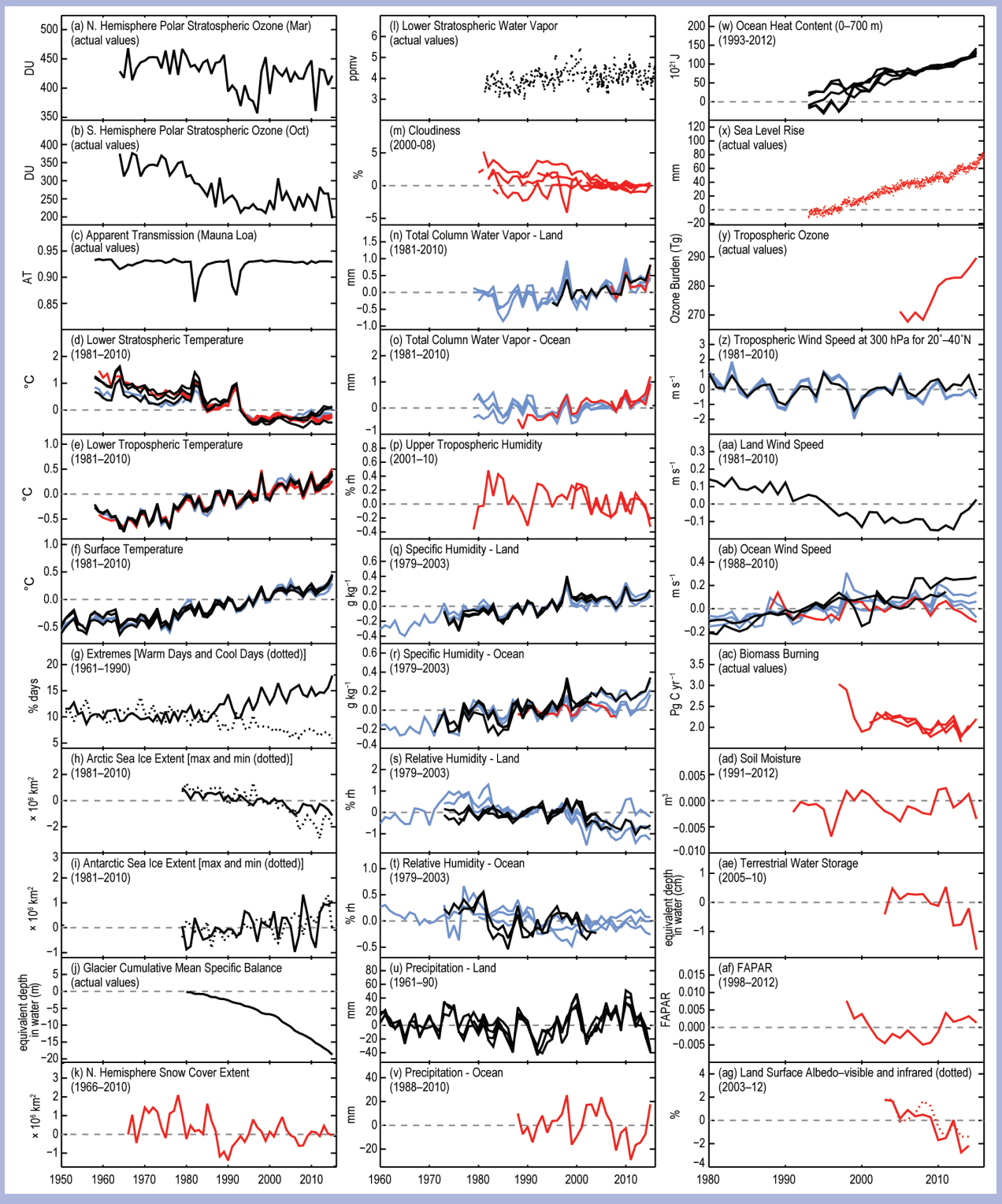
(a) N. Hemisphere Polar Stratospheric Ozone (Mar) (actual values)
DU
(b) S. Hemisphere Polar Stratospheric Ozone (Oct) (actual values)
DU
(c) Apparent Transmission (Mauna Loa) (actual values)
AT
(d) Lower Stratospheric Temperature (1981–2010)
°C
(e) Lower Tropospheric Temperature (1981–2010)
°C
(f) Surface Temperature (1981–2010)
°C
(g) Extremes [Warm Days and Cool Days (dotted)] (1961–1990)
% days
(h) Arctic Sea Ice Extent [max and min (dotted)] (1981–2010)
× 10⁶ km²
(i) Antarctic Sea Ice Extent [max and min (dotted)] (1981–2010)
× 10⁶ km²
(j) Glacier Cumulative Mean Specific Balance (actual values)
equivalent depth in water (m)
(k) N. Hemisphere Snow Cover Extent (1966–2010)
× 10⁶ km²
1950 1960 1970 1980 1990 2000 2010
(l) Lower Stratospheric Water Vapor (actual values)
ppmv
(m) Cloudiness (2000-08)
%
(n) Total Column Water Vapor - Land (1981-2010)
mm
(o) Total Column Water Vapor - Ocean (1981–2010)
mm
(p) Upper Tropospheric Humidity (2001–10)
% rh
(q) Specific Humidity - Land (1979–2003)
g kg⁻¹
(r) Specific Humidity - Ocean (1979–2003)
g kg⁻¹
(s) Relative Humidity - Land (1979–2003)
% rh
(t) Relative Humidity - Ocean (1979–2003)
% rh
(u) Precipitation - Land (1961–90)
mm
(v) Precipitation - Ocean (1988–2010)
mm
1960 1970 1980 1990 2000 2010
(w) Ocean Heat Content (0–700 m) (1993-2012)
10²¹ J
(x) Sea Level Rise (actual values)
mm
(y) Tropospheric Ozone (actual values)
Ozone Burden (Tg)
(z) Tropospheric Wind Speed at 300 hPa for 20°–40°N (1981–2010)
m s⁻¹
(aa) Land Wind Speed (1981–2010)
m s⁻¹
(ab) Ocean Wind Speed (1988–2010)
m s⁻¹
(ac) Biomass Burning (actual values)
Pg C yr⁻¹
(ad) Soil Moisture (1991–2012)
m³
(ae) Terrestrial Water Storage (2005–10)
equivalent depth in water (cm)
(af) FAPAR (1998–2012)
FAPAR
(ag) Land Surface Albedo–visible and infrared (dotted) (2003–12)
%
1980 1990 2000 2010

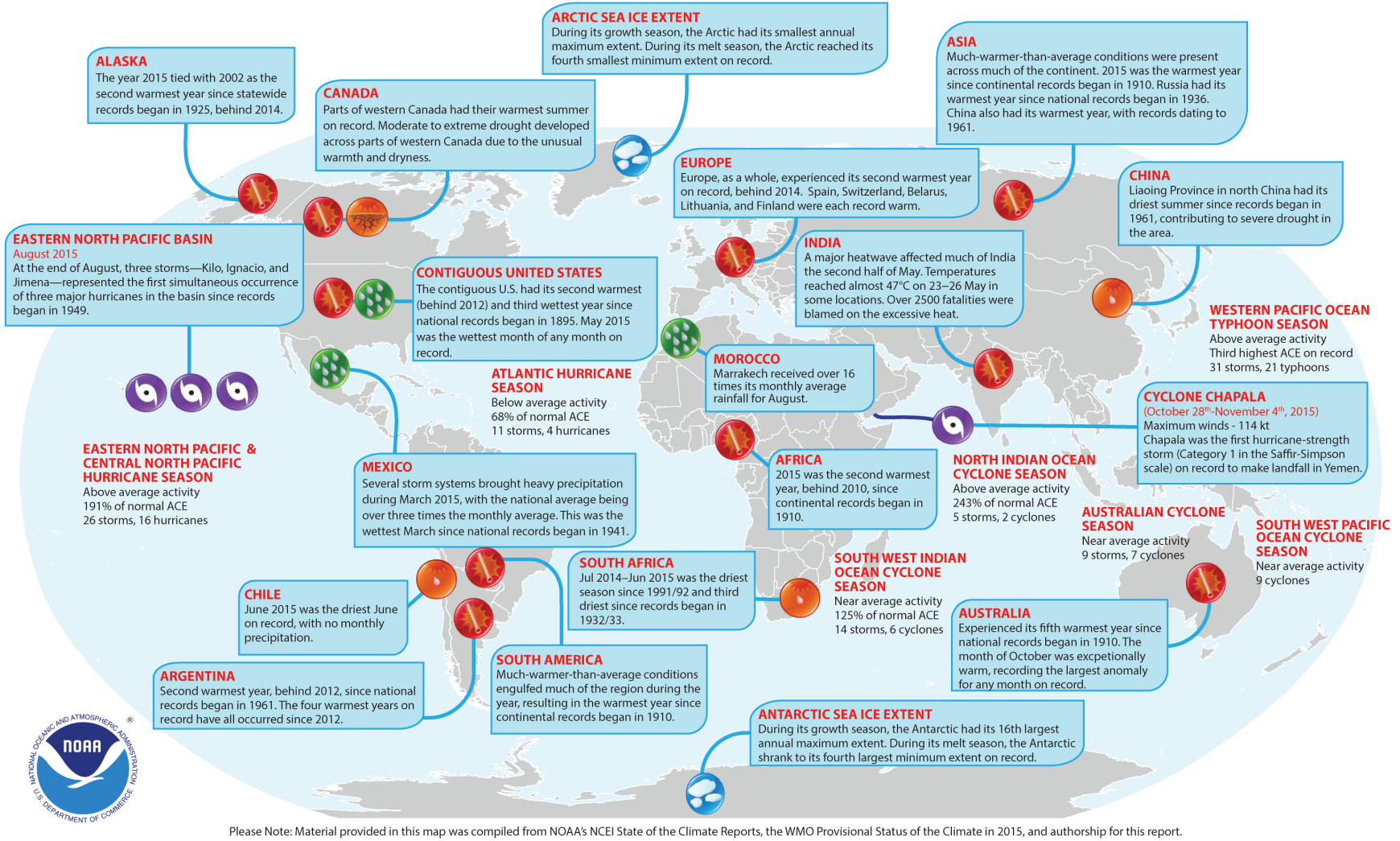

Please Note: Material provided in this map was compiled from NOAA's NCEI State of the Climate Reports, the WMO Provisional Status of the Climate in 2015, and authorship for this report.
For more information please visit: http://www.ncdc.noaa.gov/sotc

Fig. 1.1. Geographical distribution of notable climate anomalies and events occurring around the world in 2015.

SIDEBAR 1.1: THE 2015/16 EL NIÑO COMPARED WITH OTHER RECENT EVENTS—D. E. PARKER, K. M. WILLETT, R. ALLAN, C. SCHRECK, AND D. S. ARNDT

The climate of 2015 was clearly influenced by the strong 2015/16 El Niño. This sidebar places the event, still ongoing as of May 2016, into context by comparison to recent El Niños of similar magnitude.

Primary indicators of ENSO are predominantly based on SST and surface pressure changes from across the Indo-Pacific region. By most measures, the 2015/16 El Niño was one of the strongest on record, on par with those of 1982/83 and 1997/98. Figure SB1.1 shows the time evolution of tropical Pacific SSTs (from HadISST1.1) since 1970. The SST imprint for each event is unique. For example, the strongest SST anomalies in 2009/10 occurred in the central Pacific, while those for 2015/16, 1997/98, and 1982/83 were strongest in the eastern Pacific. The 2015/16 event stands as one of the more protracted warm events, with warm anomalies first appearing in summer 2014 and becoming firmly established in spring 2015.

Regionally-averaged SST anomalies (Fig. SB1.2) highlight the 2015/16 event's position among the most intense El Niño events. Notably, the Niño-4 index reached a record +1.8°C during November 2015. The 2015/16 event was only the third since 1980 (following 1982/83 and 1997/98) to exceed +2.0°C in the Niño-3, Niño-3.4, and Niño-1+2 regions; however, across Niño-1+2, the 2015/16 event, while quite strong, was almost 2°C weaker than the two strongest events: 1982/83 and 1997/98.

The 2015/16 El Niño appeared in the Southern Oscillation index (SOI; sea level pressure difference between Darwin and Tahiti; section 2e1, Fig. 2.30a,b, Fig. 4.1b) early in 2014, maturing in early 2015 and continuing into 2016. By this measure, it is a protracted event (Allan and D'Arrigo 1999). However, many other indicators are in use, reflecting the large variation in duration and character of each event. The oceanic Niño index (ONI; seasonal 3-month average of Niño-3.4 SSTs) and the Equatorial Southern Oscillation index (EQ-SOI; surface pressure difference between Indonesia and the eastern equatorial Pacific) showed neutral conditions until early 2015 (section 4b; Fig. 4.1). The Niño-3 and 3.4 regions, although mostly warm during 2014, were neither consistently nor significantly warmer than the designated threshold until early 2015 (sections 3b, 4b; Fig. 4.3). Nevertheless the protracted warmth over the tropical Pacific is clear from early 2014 onwards, as is the very different nature of each preceding El Niño event and its wider influence on climate.

El Niño events tend to elevate global mean surface temperatures and, indeed, 2015 reached record warmth (section 2b1). The history of these events since the mid-20th century in relation to global surface temperature suggests that the ongoing event will likely have a slightly greater effect on the global surface temperature of 2016 than on that of 2015.

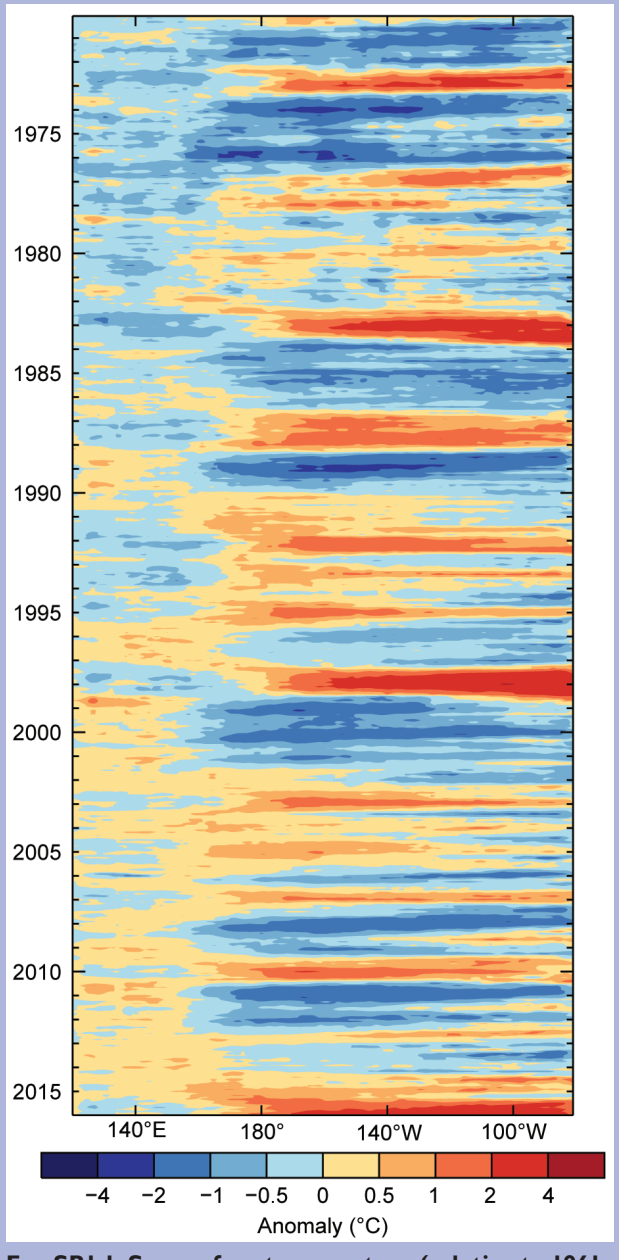

Fig. SB1.1. Sea surface temperature (relative to 1961–90 base period) averaged between 5°S and 5°N over the Pacific from 120°E to 80°W, based on HadISST1.1 (Rayner et al. 2003).

CONT. SIDEBAR 1.1: THE 2015/16 EL NIÑO COMPARED WITH OTHER RECENT EVENTS—D. E. PARKER, K. M. WILLETT, R. ALLAN, C. SCHRECK, AND D. S. ARNDT

Subsurface ocean temperature anomalies along the equatorial Pacific show significant El Niño characteristics from March–May onwards (section 4b1; Fig. 4.6). Compared to 1997 (which predated the ARGO float network) the precursor (January) warmth near the thermocline was much weaker, but the anomalies nearer the surface in December were of similar magnitude (Online Fig. S1.1).

Characteristic weakening/reversal of easterlies in the equatorial central Pacific was evident in the 2015 annual average surface winds (Plate 2.1s) with a similar signal at 850 hPa (Plate 2.1r). In late 2015 when El Niño was strongest, the negative wind anomaly in the tropical Pacific did not extend as far eastward as in late 1997, and the patterns were much less organized in the Indian and Atlantic Oceans (Online Fig. S2.22).

During El Niño events, cooling (warming) of the ocean surface and subsurface in the western (eastern) tropical Pacific, in addition to reduced drag on the ocean surface by weakened easterly winds, drives sea level fall (rise) in the western (eastern) tropical Pacific. The net effect is an increase in global sea level (section 4f; Fig. 3.17), evident in both 1997/98 and 2015/16.

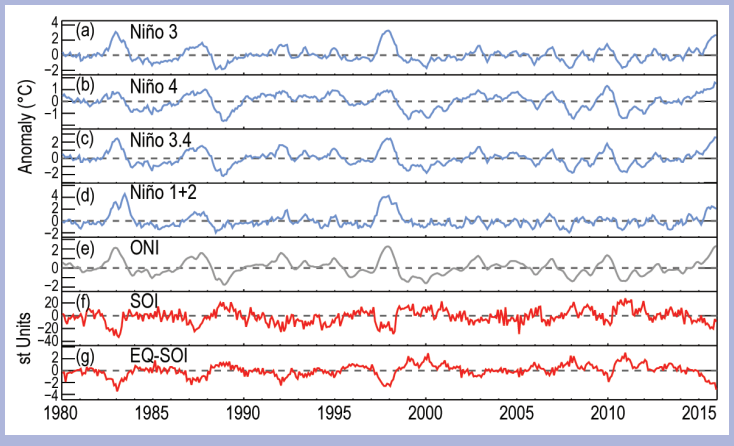

FIG. SB1.2. Time series of various ENSO indicators: (a) Niño-3: 5°S–5°N, 150°–90°W; (b) Niño-4: 5°S–5°N, 160°E–150°W; (c) Niño-3.4: 5°S–5°N, 170°–120°W; (d) Niño-1+2: 10°S–0°, 90°–80°W; (e) oceanic Niño index (ONI); (f) Southern Oscillation index (SOI); (g) Equatorial Southern Oscillation index (EQ-SOI). The Niño region time series are from HadISST1.1 (Rayner et al. 2003). The ONI and EQ-SOI are from the NOAA Climate Prediction Center (www.cpc.ncep.noaa.gov/data/indices/). The SOI is from the Australian Bureau of Meteorology.

Similar to other major El Niños, the 2015/16 event affected many parts of the global climate. Tropical cyclone activity, with respect to accumulated cyclone energy (ACE), was suppressed in the Atlantic Ocean (section 4e2) but enhanced across the North Pacific regarding both ACE and number of storms (sections 4e3, 4e4) The central Pacific was particularly active, setting several records. Global rainfall patterns were also greatly impacted (Section 4d1). The equatorial Pacific, Gulf of Mexico, and South America saw enhanced rainfall. Meanwhile, southern Africa, Australia, the Amazon, Caribbean, and Central America saw decreased rainfall. These patterns led to a substantial increase in the global land area covered by severe or extreme drought in 2015, similar to 1982/83 but not 1987/88 or 1997/98, possibly owing to countervailing influences such as extratropical atmospheric circulation patterns (section 2d9; Fig. 2.28; Plate 2.1f; Fig. 2.29).

The warmth in 2015 enabled an increase in total column water vapor (TCWV) of ~1 mm globally over both land and ocean (section 2d2; Figs. 2.16, 2.17). There were broadly similar increases following 1987/88, 1997/98, and 2009/10. Over the Pacific, 2015 lacked the dry anomaly north of the equator present in 1997 (Online Fig. S2.13). The dry anomaly over the Maritime Continent extended much farther west in 1997.

Although global average total cloudiness did not change in 2015 and shows no clear ENSO signal (Fig. 2.20), there was a dramatic shift of ice cloud from the warm pool region of the western Pacific to the central Pacific during 2015, and likewise during 1997 (section 2d4; Fig. 2.21). This shift followed the displacement of convection during the events. The eastward displacement was greater in 1997/98, matching that event's more eastward peak SST anomaly. Related regional features are apparent in 2015 annual averages of many hydrological cycle ECVs (Plate 2.1).

The tendency for increased drought in the tropics during El Niño leads to increased release of CO_2 from increased tropical wildfires. In 2015, out-of-control agricultural biomass burning was exacerbated in Indonesia (see Sidebar 2.2) by ignition of the subsurface peat. These changes in terrestrial carbon storage likely contributed to the record 3.1 ppm increase in atmospheric CO_2 at Mauna Loa Observatory from 1 January 2015 to 1 January 2016. The previous highest annual increase of 2.9 ppm occurred in 1998.

Biomass burning in Indonesia also led to regional increases in atmospheric carbon monoxide, aerosols, and tropospheric ozone in 2015 (Sidebar 2.2). Huijnen et al. 2016 suggest that the 2015 carbon emissions from the Indonesian fires were the largest since those during the El Niño year of 1997 (section 2g7; Fig. 2.60), although still only 25% of the 1997 emissions.